

Freie Universität  Berlin

---

Department of Physics  
Freie Universität Berlin  
Arnimallee 14  
14195 Berlin, Germany

# Parametric Destabilisation for Collective Oscillations in Ultracold Bose Gases

by Jochen Brüggemann

Supervisor: Priv.-Doz. Dr. Axel Pelster

September 30th, 2009

# Contents

<b>1</b>	<b>Introduction</b>	<b>3</b>
<b>2</b>	<b>Dynamics of a Bose-Einstein Condensate in a Trap</b>	<b>5</b>
2.1	Gross-Pitaevskii Equation and Variational Principle . . . . .	5
2.2	Equilibrium Positions . . . . .	9
2.3	Collective Oscillations . . . . .	11
2.4	Discussion . . . . .	16
<b>3</b>	<b>Parametric Resonance</b>	<b>16</b>
3.1	Spherical Trap . . . . .	17
3.2	Pendulum . . . . .	18
3.3	Floquet Theory . . . . .	18
3.4	Fourier Series . . . . .	19
3.5	Stability Borders . . . . .	21
3.6	Resonance Curves . . . . .	23
<b>4</b>	<b>Summary and Conclusion</b>	<b>26</b>

---

# 1 Introduction

In 1924 Satyendra Nath Bose sent a paper investigating the statistics of photons to Albert Einstein. Shortly after that Einstein generalised the idea from massless to massive particles and predicted that for a system of weakly or non-interacting bosons a phase transition would occur at very low temperatures, leading to a macroscopic occupation of the ground state [1,2]. About 70 years later, due to new cooling techniques based on laser technology and evaporative cooling, it was possible to create the Bose-Einstein condensate under laboratory conditions [3,4]. Since then there has been a lot of research on this topic [5–8]. Both the dynamics - mostly at zero temperature - and the thermodynamical properties are topics of high interest for experimental as well as theoretical physicists.

Regarding the dynamics of the condensate it is possible to analyse collective oscillations which are not only easily produced in the experiments but can also be measured within a very high accuracy leading to an error of less than 1 percent [9]. They are described theoretically by the time-dependent Gross-Pitaevskii equation, which describes the condensate at zero temperature. Within the thermodynamic limit this equation can be approximately solved in the Thomas-Fermi regime where the kinetic term is neglected in comparison with the interaction. Using this approximation the excitation spectrum of a condensate in a harmonic trap has been derived already by Stringari [10]. A more general solution for a finite particle number can be derived within a variational ansatz [11,12] and leads to results for both repulsive as well as attractive interactions. The latter will be used in this work where we analyse collective oscillations of a trapped condensate under the influence of a parametric oscillation. Usually the different oscillation modes of a trapped BEC are excited by small changes of the trap geometry. In this way it is possible to excite the dipole as well as the quadrupole mode. However, the excitation analysed in this work will not be caused by changing the trap symmetry. Instead the s-wave scattering length of the condensate will be modified by applying an external oscillating magnetic field via Feshbach resonance [13] shown in Figure 1. Parametric resonance is a phenomenon that arises when a former time-independent parameter of an oscillating system periodically changes with time (see, for instance, Ref. [14]). In this case resonances can be observed. It is possible to stabilise or destabilise the oscillations of the system in this way. One of the most common applications for parametric resonance is the Paul-trap [15] which is used to store charged particles by using alternating electrical fields.

Currently there is an experimental group led by V.S. Bagnato and R.G. Hulet that excites the quadrupole collective mode of a trapped Bose-gas by applying a Feshbach resonance [16]. The experiment is done in the following way: A BEC of  ${}^7\text{Li}$  is produced by Zeeman decelerating the atoms and confining them in an optical trap. Coaxial to the trap laser there are coils which allow to manipulate the s-wave scattering length. In the first step the scattering length has to be large in order to accelerate the thermalisation of the atoms and enhancing the evaporation process. After obtaining a condensate of about  $10^5$  atoms the magnetic field is lowered slowly to the desired value. The modulation of the scattering length is now realised by adding a small AC component to the bias field of the trap:

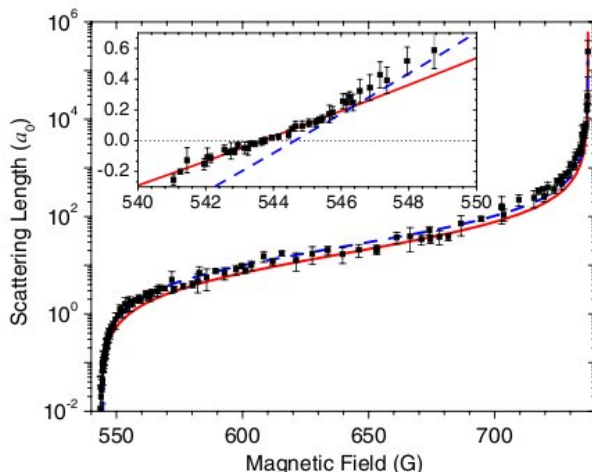


Figure 1: Dependence of the s-wave scattering length from an external magnetic field for  ${}^7\text{Li}$  atoms. Since the function diverges at a special point it is possible to obtain any desired value for the scattering length [13].

$$B(t) = B_0 + b \cos \Omega t, \quad (1)$$

with an average magnetic field  $B_0 = 565$  G and a modulation of  $b \simeq 10$  G. Thus the scattering length reads

$$a_s(t) = a_{\text{nr}} \left[ 1 - \frac{\Delta}{B(t) - B_{\text{res}}} \right], \quad (2)$$

where  $a_{\text{nr}} = -24.5 a_0$  ( $a_0$  being the Bohr radius) denotes the non-resonant scattering length,  $B_{\text{res}} = 736.8$  G the resonant field value for  $a_s$ , and  $\Delta = 192.3$  G is the resonance width. For sufficiently small amplitude  $b$  Eq. (2) reduces to

$$a_s(t) \simeq a_{\text{av}} + a \cos \Omega t \quad (3)$$

with the average scattering length  $a_{\text{av}} \simeq 2.9 a_0$  and the amplitude  $a \simeq -1.6 a_0$ . The experiment is performed for different modulation frequencies  $\Omega$  in such a way that an image of the condensates' radius over the modulation frequency is obtained.

Figure 2 shows the results of the ongoing experiment [16]. The harmonic trap used in the experiment is cylindric with the two trap frequencies  $\omega_z = 2\pi \times 5.5$  Hz and  $\omega_r = 2\pi \times 255$  Hz. For the quadrupole mode the oscillation of the cloud radius was observed in dependency of the modulation frequency. A big resonance peak can be found at a modulation frequency around 9 Hz and a smaller one around the doubled value of 18 Hz. The grey line shows a numerical simulation of the spectrum for a quadrupole mode. The resonance peaks denote a destabilisation of the eigenmode of the condensate. Such a destabilisation is the main topic in this work which will describe a similar system from a theoretical point of view. In contrary to the experiment here the condensate will be confined in a trap with spherical symmetry, which simplifies the complexity of the problem. In this case stabilisation and

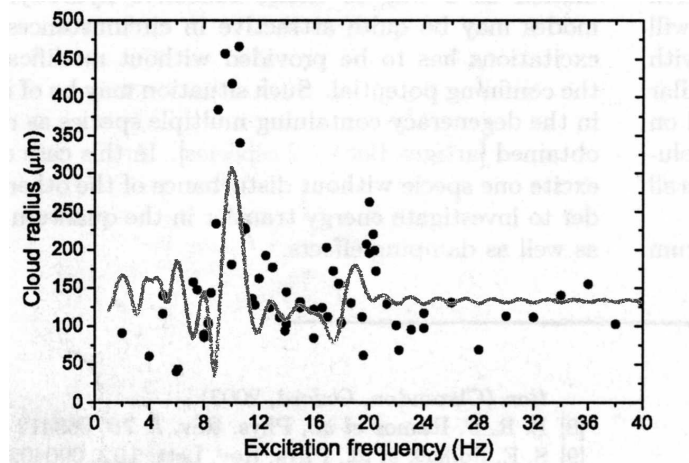


Figure 2: Resonance spectrum obtained by the experiment led by V.S. Bagnato and R.G. Hulet as well as a numerical simulation of the experiment [16]. The amplitude of the condensates oscillation has been determined depending on the modulation frequency  $\Omega$  for a fixed average scattering length  $a_{av}$  and scattering length amplitude  $a$ .

destabilisation for the breathing mode can be discussed. A similar study has been performed in [17,18] with other methods. The outline of the thesis is as follows. In the second chapter the dynamics of a condensate in a harmonic trap will be examined. The third section will concentrate on the phenomenon of parametric resonance by deriving the characteristic properties for the Mathieu equation and then applying those properties on the collective oscillations of the condensate which are described by the Mathieu equation.

## 2 Dynamics of a Bose-Einstein Condensate in a Trap

In this section the time-dependent Gross-Pitaevskii equation will be solved with a Gaussian trial function depending on six variational parameters. This will lead to a set of ordinary differential equations which describe the dynamics of the condensate via its widths. The resulting equilibrium positions will be discussed as well as the collective oscillations of the condensate in the vicinity of these positions and the corresponding eigenmodes. The latter are of further interest in this work because they are to be stabilised or destabilised via parametric resonance.

### 2.1 Gross-Pitaevskii Equation and Variational Principle

The dynamics of a condensed Bose gas in a trap at zero temperature is described by the time-dependent Gross-Pitaevskii equation, often called nonlinear Schrödinger equation,

$$i\hbar \frac{\partial}{\partial t} \Psi(\mathbf{x}, t) = \left\{ -\frac{\hbar^2}{2M} \Delta + V(\mathbf{x}) + g(t) |\Psi(\mathbf{x}, t)|^2 \right\} \Psi(\mathbf{x}, t), \quad (4)$$

with the harmonic trap potential

$$V(\mathbf{x}) = \frac{M}{2} \sum_{i=1}^3 \omega_i^2 x_i^2 \quad (5)$$

and the parameter  $g$  describing the strength of the two-particle interaction

$$g(t) = \frac{4\pi\hbar^2 a(t)}{M}, \quad (6)$$

where  $a(t)$  denotes the s-wave scattering length from (3).

There are two essential points where (4) differs from the Schrödinger equation. The first one is the non-linear interaction term  $g(t) |\Psi(\mathbf{x}, t)|^2 \Psi(\mathbf{x}, t)$ . Additionally the wave function  $\Psi(\mathbf{x}, t)$  is not normalised to 1 but to the total particle number  $N$  of our Bose gas:

$$N = \int d^3x |\Psi(\mathbf{x}, t)|^2. \quad (7)$$

The time-dependent Gross-Pitaevskii equation follows from the action

$$\mathcal{A}[\Psi^*, \Psi] = \int dt \int d^3x \mathcal{L} \left( \Psi^*(\mathbf{x}, t), \nabla \Psi^*(\mathbf{x}, t), \frac{\partial \Psi^*(\mathbf{x}, t)}{\partial t}; \Psi(\mathbf{x}, t), \nabla \Psi(\mathbf{x}, t), \frac{\partial \Psi(\mathbf{x}, t)}{\partial t} \right) \quad (8)$$

with the Lagrange density

$$\begin{aligned} \mathcal{L} = & i\hbar \Psi^*(\mathbf{x}, t) \frac{\partial \Psi(\mathbf{x}, t)}{\partial t} - \frac{\hbar^2}{2M} \nabla \Psi^*(\mathbf{x}, t) \nabla \Psi(\mathbf{x}, t) \\ & - V(\mathbf{x}) \Psi^*(\mathbf{x}, t) \Psi(\mathbf{x}, t) - \frac{g(t)}{2} \Psi^*(\mathbf{x}, t)^2 \Psi(\mathbf{x}, t)^2. \end{aligned} \quad (9)$$

This indeed leads to the Gross-Pitaevskii equation (4) if applied to the Hamilton's principle

$$\delta \mathcal{A}[\Psi^*, \Psi] = 0 \quad (10)$$

yielding the Euler-Lagrange equation

$$\frac{\delta \mathcal{A}}{\delta \Psi^*(\mathbf{x}, t)} = \frac{\partial \mathcal{L}}{\partial \Psi^*(\mathbf{x}, t)} - \nabla \frac{\partial \mathcal{L}}{\partial \nabla \Psi^*(\mathbf{x}, t)} - \frac{\partial}{\partial t} \frac{\partial \mathcal{L}}{\partial \frac{\partial \Psi^*(\mathbf{x}, t)}{\partial t}} = 0, \quad (11)$$

and its complex conjugate. Now we follow Ref. [11] and use the Gaussian trial function

$$\Psi(\mathbf{x}, t) = \frac{N^{1/2}}{\pi^{3/4} \tilde{A}(t)^{3/2}} \exp \left\{ - \sum_{i=1}^3 \left[ \frac{1}{2A_i(t)^2} + iB_i(t) \right] x_i^2 \right\} \quad (12)$$

with  $\tilde{A}(t)^3$  being the product over all  $A_i(t)$ . Thus the Langrange function

$$L = \int d^3x \mathcal{L} \quad (13)$$

can be calculated by inserting (12) in (8) and (9). The result is the action as a functional of the variational parameters  $A_i(t)$  and  $B_i(t)$ .

The Lagrange function can be split into four parts which are now to be calculated separately:

$$L = L_{\text{time}} + L_{\text{kin}} + L_{\text{pot}} + L_{\text{int}}. \quad (14)$$

The potential part

$$L_{\text{pot}} = - \int d^3x V(\mathbf{x}) |\Psi(\mathbf{x}, t)|^2 \quad (15)$$

gives

$$L_{\text{pot}} = - \frac{NM}{4} \sum_{i=1}^3 \omega_i^2 A_i^2(t). \quad (16)$$

The part describing the interaction

$$L_{\text{int}} = - \frac{g(t)}{2} \int d^3x |\Psi(\mathbf{x}, t)|^4 \quad (17)$$

leads to

$$L_{\text{int}} = - \frac{g(t) N^2}{2(2\pi)^{3/2} \tilde{A}(t)^3}. \quad (18)$$

In the same way it is possible to calculate the kinetic part

$$L_{\text{kin}} = - \frac{\hbar^2}{2M} \int d^3x \nabla \Psi^*(\mathbf{x}, t) \nabla \Psi(\mathbf{x}, t), \quad (19)$$

yielding

$$L_{\text{kin}} = -N \sum_{i=1}^3 \left\{ \frac{\hbar^2}{4M A_i^2(t)} + \frac{\hbar^2}{M} B_i^2(t) A_i^2(t) \right\} \quad (20)$$

by evaluating the Gauss integrals. The last part

$$L_{\text{time}} = -i\hbar \int d^3x \Psi^*(\mathbf{x}, t) \frac{\partial \Psi(\mathbf{x}, t)}{\partial t} \quad (21)$$

becomes

$$L_{\text{time}} = \frac{N\hbar}{2} \sum_{i=1}^3 A_i^2(t) \dot{B}_i(t). \quad (22)$$

Inserting these results into (14) finally leads to the Lagrange function

$$L = N \sum_{i=1}^3 \left\{ \frac{\hbar}{2} A_i^2(t) \dot{B}_i(t) - \frac{\hbar^2}{4M A_i^2(t)} - \frac{\hbar^2}{M} B_i^2(t) A_i^2(t) - \frac{M}{4} \omega_i^2 A_i^2(t) \right\} - \frac{g(t)N^2}{2(2\pi)^{3/2} \tilde{A}(t)^3}, \quad (23)$$

and the corresponding action is defined by

$$\mathcal{A}[A_i, B_i] = \int dt L \left( A_i(t), \dot{A}_i(t); B_i(t), \dot{B}_i(t) \right). \quad (24)$$

In analogy to Ritz' variational principle an expression for the variational parameters can be found by extremising (24) with respect to the variational parameters  $A_i(t)$  and  $B_i(t)$ . This leads to the Euler-Lagrange equations

$$\frac{\partial L}{\partial A_i(t)} - \frac{d}{dt} \frac{\partial L}{\partial \dot{A}_i(t)} = 0, \quad (25)$$

$$\frac{\partial L}{\partial B_i(t)} - \frac{d}{dt} \frac{\partial L}{\partial \dot{B}_i(t)} = 0. \quad (26)$$

The first one reads

$$-\hbar A_i(t) \dot{B}_i(t) + \frac{2\hbar^2}{M} B_i^2(t) A_i(t) + \frac{M}{2} \omega_i^2 A_i(t) = \frac{\hbar^2}{2M A_i^3(t)} + \frac{g(t)N}{2(2\pi)^{3/2} \tilde{A}(t)^3 A_i(t)}, \quad (27)$$

whereas the second one turns out to be

$$B_i(t) = -\frac{M \dot{A}_i(t)}{2\hbar A_i(t)}. \quad (28)$$

Inserting (28) into (27) leads to

$$\ddot{A}_i(t) + \omega_i^2 A_i(t) = \frac{\hbar^2}{2M A_i^3(t)} + \frac{g(t)N}{(2\pi)^{3/2} M \tilde{A}(t)^3 A_i(t)}. \quad (29)$$

Notice that the dynamics is essentially due to the variational parameters  $B_i(t)$ . With only  $A_i(t)$  as variational parameters the procedure would not have resulted in equations of motion. Before discussing

them further, it is rather useful to introduce dimensionless variables

$$\omega_i = \lambda_i \omega, \quad A_i = \sqrt{\frac{\hbar}{M\omega}} \alpha_i, \quad \tau = \omega t \quad (30)$$

and to make use of (6) in order to introduce the dimensionless coupling strength

$$P(\tau) = \sqrt{\frac{2}{\pi}} \frac{a(\tau)N}{\sqrt{\hbar/M\omega}}. \quad (31)$$

This results in a system of three coupled ordinary differential equations describing the dynamics of the condensate via its widths:

$$\ddot{\alpha}_x(\tau) + \lambda_x^2 \alpha_x(\tau) = \frac{1}{\alpha_x^3(\tau)} + \frac{P(\tau)}{\alpha_x^2(\tau)\alpha_y(\tau)\alpha_z(\tau)}, \quad (32)$$

$$\ddot{\alpha}_y(\tau) + \lambda_y^2 \alpha_y(\tau) = \frac{1}{\alpha_y^3(\tau)} + \frac{P(\tau)}{\alpha_y^2(\tau)\alpha_x(\tau)\alpha_z(\tau)}, \quad (33)$$

$$\ddot{\alpha}_z(\tau) + \lambda_z^2 \alpha_z(\tau) = \frac{1}{\alpha_z^3(\tau)} + \frac{P(\tau)}{\alpha_z^2(\tau)\alpha_x(\tau)\alpha_y(\tau)}. \quad (34)$$

Those equations of motion correspond to harmonic oscillators modified by a kinetic term and an additional term that depends on the dimensionless parameter  $P(\tau)$  which describes according to (31) the strength of the interaction between particles in the condensate and depends on the s-wave scattering length  $a(\tau)$ . In the introduction it is described how the oscillation of  $a(\tau)$  is introduced and that is expressed for small amplitudes according to (3). Thus it is useful to split  $P(\tau)$  into a constant and an oscillating part

$$P(\tau) = P_0 + P_1 \cos \frac{\Omega\tau}{\omega}. \quad (35)$$

The dimensionless interaction parameters  $P_0$  and  $P_1$  are given by (31) with the values for  $a_{av}$  and  $a$  mentioned in the introduction (3). Since those parameters are constant in the experiment the only control parameter in the following is the modulation frequency  $\Omega$ .

## 2.2 Equilibrium Positions

Taking another look at the equations of motion (32)–(34) reveals that the dynamics of the widths of the condensate can be described as the motion of a point mass according to

$$\ddot{\alpha}_i(\tau) = -\frac{\partial V_{\text{eff}}(\alpha_x(\tau), \alpha_y(\tau), \alpha_z(\tau))}{\partial \alpha_i(\tau)}, \quad (36)$$

where the effective potential is given by

$$V_{\text{eff}}(\alpha_x, \alpha_y, \alpha_z) = \sum_{i=1}^3 \frac{1}{2} \left( \lambda_i^2 \alpha_i^2 + \frac{1}{\alpha_i^2} \right) + \frac{P(\tau)}{\alpha_x \alpha_y \alpha_z}. \quad (37)$$

Thus, the equilibrium positions are calculated by setting the gradient of the potential to zero and by neglecting the time dependency of  $P(\tau)$ , which yields

$$\lambda_x^2 \alpha_{x0} = \frac{1}{\alpha_{x0}^3} + \frac{P_0}{\alpha_{x0}^2 \alpha_{y0} \alpha_{z0}}, \quad (38)$$

$$\lambda_y^2 \alpha_{y0} = \frac{1}{\alpha_{y0}^3} + \frac{P_0}{\alpha_{y0}^2 \alpha_{x0} \alpha_{z0}}, \quad (39)$$

$$\lambda_z^2 \alpha_{z0} = \frac{1}{\alpha_{z0}^3} + \frac{P_0}{\alpha_{z0}^2 \alpha_{x0} \alpha_{y0}}. \quad (40)$$

Specialising to cylindrical symmetry according to  $\alpha_{x0} = \alpha_{y0} = \alpha_0$ , this leads to the two algebraic equations

$$\alpha_0^4 = 1 + \frac{P_0}{\alpha_{z0}}, \quad (41)$$

$$\lambda^2 \alpha_{z0}^4 = 1 + \frac{P_0 \alpha_{z0}}{\alpha_0^2} \quad (42)$$

for the equilibrium positions  $\alpha_0$  and  $\alpha_{z0}$ .

Since the dynamics of the condensate will evolve around the equilibrium positions in this work, it is convenient to analyse their position and stability. This can be done by finding a single equation for  $\alpha_{z0}$  depending on  $P_0$ . Solving (42) for  $\alpha_0^2$  and inserting the result into (41) leads to

$$\lambda^4 \alpha_{z0}^9 \left( 1 + \frac{P_0}{\alpha_{z0}} \right) - 2\lambda^2 \alpha_{z0}^5 \left( 1 + \frac{P_0}{\alpha_{z0}} \right) - P_0^2 \alpha_{z0}^3 + \alpha_{z0} - P_0 = 0, \quad (43)$$

which represents a polynomial of ninth degree in  $\alpha_{z0}$ . It is important to notice that there may be fake solutions because of squaring (41) in the beginning of the calculations. Therefore it is necessary to check for every solution of (43) whether it also solves (41) and (42).

The sought solutions are the real, positive zeros of the polynomial (43) since neither a negative nor an imaginary width does hold any physical meaning. The number of those solutions turns out to depend on  $P_0$ .

This work will be based on a condensate in a trap with spherical symmetry where the calculation of the equilibrium positions and their stability becomes much easier. Setting  $\lambda = 1$  and  $\alpha_{z0} = \alpha_0$  reduces the equilibrium equations (41) and (42) to

$$\alpha_0^5 - \alpha_0 - P_0 = 0. \quad (44)$$

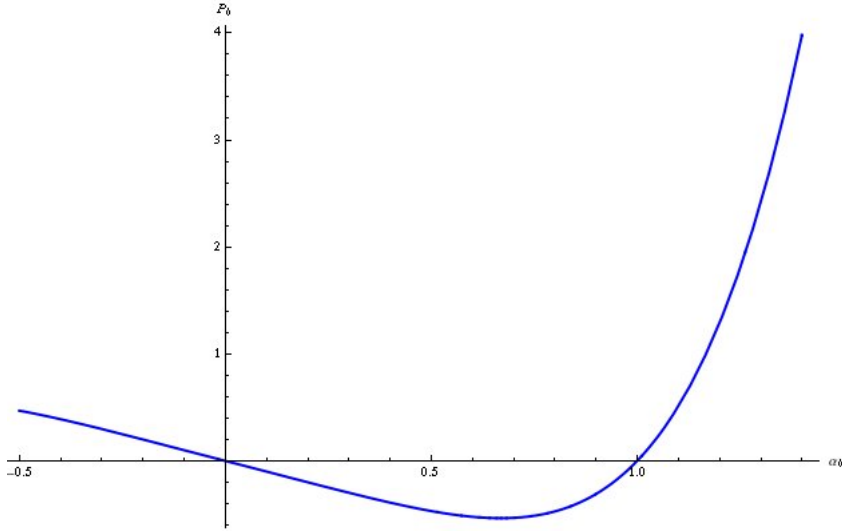


Figure 3: Dimensionless interaction strength  $P_0$  as a function of the variational width parameter  $\alpha_0$ . There is a minimum for  $P_0 = P_{\text{crit}}$ . The condensate will collapse for all values smaller than this critical  $P_{\text{crit}}$ .

For different values of  $P_0$  there are either 0, 1 or 2 real, positive solutions. There is no equilibrium point for all values of  $P_0$  lower than

$$P_{\text{crit}} = \left(\frac{-4}{5}\right) \frac{1}{5^{1/4}} \simeq -0.535. \quad (45)$$

All positive values of  $P_0$  lead to one solution. Particular interesting is the stability of the two solutions which exist for  $0 > P_0 > P_{\text{crit}}$ , which can be seen in Figure 3 because both stable and unstable solutions are to be expected there. In order to determine the stability of the solutions, the oscillation frequencies of the isotropic condensate around these certain equilibrium points have to be calculated.

### 2.3 Collective Oscillations

The current task is to solve (32)–(34) in the vicinity of  $(\alpha_{x0}, \alpha_{y0}, \alpha_{z0})$ . For small deflections  $\delta\alpha_i$  from the equilibrium position, the potential can be expanded into a Taylor series:

$$V_{\text{eff}}(\alpha_{x0} + \delta\alpha_x, \alpha_{y0} + \delta\alpha_y, \alpha_{z0} + \delta\alpha_z) = V_{\text{eff}}(\alpha_{x0}, \alpha_{y0}, \alpha_{z0}) + \sum_{i=1}^3 \left( \frac{\lambda_i^2}{2} + \frac{3}{2\alpha_{i0}^4} + \frac{P(\tau)}{\alpha_{i0}^2 \alpha_{x0} \alpha_{y0} \alpha_{z0}} \right) \delta\alpha_i^2 + \frac{P(\tau)}{\alpha_{x0} \alpha_{y0} \alpha_{z0}} \left( \frac{\delta\alpha_x \delta\alpha_y}{\alpha_{x0} \alpha_{y0}} + \frac{\delta\alpha_y \delta\alpha_z}{\alpha_{y0} \alpha_{z0}} + \frac{\delta\alpha_x \delta\alpha_z}{\alpha_{x0} \alpha_{z0}} \right) + \dots, \quad (46)$$

which, in case of the axial symmetry, can be written as

$$V_{\text{eff}}(\alpha_0 + \delta\alpha_x, \alpha_0 + \delta\alpha_y, \alpha_{z0} + \delta\alpha_z) = V_{\text{eff}}(\alpha_0, \alpha_{z0}) + \frac{1}{2} \delta\boldsymbol{\alpha}^T M(\tau) \delta\boldsymbol{\alpha} + \dots, \quad (47)$$

with  $\delta\boldsymbol{\alpha}^T = (\delta\alpha_x, \delta\alpha_y, \delta\alpha_z)$  and

$$M(\tau) = \begin{pmatrix} 1 + \frac{3}{\alpha_0^4} + \frac{2P(\tau)}{\alpha_0^4 \alpha_{z0}} & \frac{P(\tau)}{\alpha_0^4 \alpha_{z0}} & \frac{P(\tau)}{\alpha_0^3 \alpha_{z0}^2} \\ \frac{P(\tau)}{\alpha_0^4 \alpha_{z0}} & 1 + \frac{3}{\alpha_0^4} + \frac{2P(\tau)}{\alpha_0^4 \alpha_{z0}} & \frac{P(\tau)}{\alpha_0^3 \alpha_{z0}^2} \\ \frac{P(\tau)}{\alpha_0^3 \alpha_{z0}^2} & \frac{P(\tau)}{\alpha_0^3 \alpha_{z0}^2} & \lambda^2 + \frac{3}{\alpha_{z0}^4} + \frac{2P(\tau)}{\alpha_0^2 \alpha_{z0}^3} \end{pmatrix}. \quad (48)$$

Thus the dynamics for small deflections around the equilibrium positions is described by oscillations with the amplitudes  $\delta\alpha_i$ . In the following it has to be analysed if the oscillation frequencies are real, complex or even pure imaginary, which would lead to non-stable equilibrium points. Additionally it is possible to determine the oscillation modes once the frequencies are known.

The frequencies are related to the eigenvalues of the matrix  $M_{(0)}$ , which is obtained from (48) by replacing  $P(\tau)$  with  $P_0$ . The eigenvalue problem reads

$$(M_{(0)} - \xi I) \mathbf{x} = 0, \quad (49)$$

which will finally lead to the oscillation frequencies  $\nu = \omega\sqrt{\xi}$  and by calculating the eigenvectors  $\mathbf{x}$  will allow to determine the different eigenmodes.

The characteristic polynomial corresponding to  $M_{(0)}$  is

$$p(\xi) = A^2 \cdot C + D \cdot B - B \cdot A - C \cdot D^2, \quad (50)$$

with the abbreviations

$$A = 3 + \frac{1}{\alpha_0^4} - \xi, \quad (51)$$

$$B = 2 \left( \frac{P_0}{\alpha_0^3 \alpha_{z0}^2} \right)^2, \quad (52)$$

$$C = \lambda^2 + \frac{3}{\alpha_{z0}^4} + \frac{2P_0}{\alpha_0^2 \alpha_{z0}^3} - \xi, \quad (53)$$

$$D = \frac{P_0}{\alpha_0^4 \alpha_{z0}}. \quad (54)$$

Thus the solutions are obtained by requiring  $p(\xi) = 0$ , i.e.

$$A(A \cdot C - B) - D(D \cdot C - B) = 0. \quad (55)$$

A close inspection shows that one solution is  $A = D$ , resulting in

$$\xi_a = 4 - \frac{2P_0}{\alpha_0^4 \alpha_{z0}}. \quad (56)$$

The remaining two solutions are given by the following equation which is of second degree in  $\xi$ :

$$A = \frac{B - C \cdot D}{C}. \quad (57)$$

After a few algebraic manipulations and using the constraints for the equilibrium points (41), (42) the final result is

$$\xi_{b,c} = 2 \left( 1 + \lambda^2 - \frac{P_0}{4\alpha_0^2 \alpha_{z0}^3} \right) \mp 2 \sqrt{\left( 1 - \lambda^2 + \frac{P_0}{4\alpha_0^2 \alpha_{z0}^3} \right)^2 + \frac{P_0^2}{2\alpha_0^6 \alpha_{z0}^4}}. \quad (58)$$

As already mentioned the eigenvalues correspond to oscillation frequencies for the condensate. The resulting three frequencies are [11]

$$\nu_a = 2\omega \sqrt{1 - \frac{P_0}{2\alpha_0^4 \alpha_{z0}}}, \quad (59)$$

$$\nu_{b,c} = 2\omega \left\{ \frac{1}{2} \left( 1 + \lambda^2 - \frac{P_0}{4\alpha_0^2 \alpha_{z0}^3} \right) \mp \frac{1}{2} \sqrt{\left( 1 - \lambda^2 + \frac{P_0}{4\alpha_0^2 \alpha_{z0}^3} \right)^2 + \frac{P_0^2}{2\alpha_0^6 \alpha_{z0}^4}} \right\}^{1/2}. \quad (60)$$

With this, determining the eigenmodes becomes a straight-forward but cumbersome calculation.

For the first eigenvalue  $\xi_a$  two of the matrix columns are identical.

$$A(x_1 + x_2) + Bx_3 = 0 \quad (61)$$

$$A(x_1 + x_2) + Bx_3 = 0 \quad (62)$$

$$B(x_1 + x_2) + Cx_3 = 0. \quad (63)$$

Solving this system gives

$$\mathbf{x}_a = \begin{pmatrix} 1 \\ -1 \\ 0 \end{pmatrix}, \quad (64)$$

which describes an oscillation in only  $x$  and  $y$  direction while the width  $\alpha_z$  remains unchanged, which is called 2D-quadrupole mode.

For the eigenvalue  $\xi_{b,c}$  we obtain correspondingly:

$$Ax_1 + Bx_2 + Cx_3 = 0 \quad (65)$$

$$Bx_1 + Ax_2 + Cx_3 = 0 \quad (66)$$

$$C(x_1 + x_2) + Dx_3 = 0. \quad (67)$$

Using the constraints for the equilibrium positions (41) and (42) this system of linear equations leads to:

$$\mathbf{x}_{b,c} = \begin{pmatrix} 1 \\ 1 \\ \frac{2\xi_{b,c}-8}{BD} \end{pmatrix}. \quad (68)$$

Of these two eigenmodes the first one,  $\mathbf{x}_b$ , is called stretching mode due to the negative algebraic sign of the  $z$ -component and  $\mathbf{x}_c$  is called breathing mode as it has a positive  $z$ -component.

For the parametric resonance it is important to determine which frequencies belong to stable and/or unstable oscillations. The unstable oscillations are of highest interest. If there is such an unstable oscillation mode, being able to stabilise it under certain circumstances will hold important practical applications, maybe similar to Paul-traps or other systems where parametric resonance is already in use. In order to see if this is possible, it has to be determined if the frequencies have real or complex values.

This is what will be done now for the isotropic trap, where (59) reduces to the real value

$$\nu_a = \omega \sqrt{2 + \frac{2}{\alpha_0^4}} \quad (69)$$

for any possible  $\alpha_0$ . Correspondingly we obtain from (60)

$$\nu_{b,c} = \omega \sqrt{2 \left(2 - \frac{P_0}{4\alpha_0^5}\right) \mp 2 \sqrt{\left(\frac{P_0}{4\alpha_0^5}\right)^2 + \frac{P_0^2}{2\alpha_0^{10}}}}, \quad (70)$$

$$\nu_{b,c} = \omega \sqrt{\frac{7}{2} + \frac{1}{2\alpha_0^4} \mp \frac{3}{2} \left(1 - \frac{1}{\alpha_0^4}\right)}. \quad (71)$$

Thus, the other two frequencies are

$$\nu_b = \omega \sqrt{2 + \frac{2}{\alpha_0^4}} \quad (72)$$

which, again, is a real number and actually the same as  $\nu_a$  in (69) and

$$\nu_c = \omega \sqrt{5 - \frac{1}{\alpha_0^4}}. \quad (73)$$

This last frequency will be imaginary for  $P_0 < P_{\text{crit}}$  with  $P_{\text{crit}}$  defined by (45).

It remains for us to explore the consequences of these results in two important particular cases: The Thomas-Fermi limit of large particle numbers, which occurs for the current experiment and in the case

without any interaction, both for a spherical trap which will be used for the parametric resonance later on.

In the limit  $P_0 \rightarrow \infty$  the equilibrium conditions (41) and (42) reduce to

$$P_0 = \alpha_0^4 \alpha_{z0}, \quad \lambda^2 \alpha_{z0}^2 = \alpha_0^2 \quad (74)$$

and the resulting frequencies are

$$\nu_a = \sqrt{2}\omega, \quad (75)$$

$$\nu_{b,c} = \frac{\omega}{\sqrt{2}} \left[ 4 + 3\lambda^2 \mp \sqrt{16 - 16\lambda^2 + 9\lambda^4} \right]^{1/2}. \quad (76)$$

Those values can also be deduced immediately by the Thomas-Fermi-approximation in the Gross-Pitaevskii equation which was done by Stringari in 1996 [10]. By comparing the results it is possible to assign the modes described by the different quantum numbers to the calculated frequencies. Separating the condensates density  $\delta n(r, \vartheta, \varphi)$  into a radial and an angle-dependent part

$$\delta n(r, \vartheta, \varphi) = A(r)Y_{lm}(\vartheta, \varphi) \quad (77)$$

leads to the following oscillation frequency for an isotropic trap:

$$\nu = \omega \sqrt{2n^2 + 2nl + 3n + l}, \quad (78)$$

where  $n$  denotes the main quantum number and  $l$  the quantum number for the angular momentum. In comparison to that the frequencies (75), (76) calculated for  $\lambda = 1$  are

$$\nu_{a,b} = \sqrt{2}\omega, \quad \nu_c = \sqrt{5}\omega. \quad (79)$$

Thus the comparison leads to identifying the quantum numbers  $n = 0, l = 2$  characterising quadrupole modes for the  $a$ - and  $b$ -modes as well as  $n = 1, l = 0$  which denotes a monopole mode for the  $c$ -mode.

The other limit  $P_0 \rightarrow 0$  reduces the Gross-Pitaevskii equation to a simple Schrödinger equation. In this case the frequencies are straight-forward to calculate. The energy levels are given by

$$E_{n,l} = \hbar\omega \left( 2n + l + \frac{3}{2} \right), \quad (80)$$

with the ground state energy  $E_{0,0} = \frac{3}{2}\hbar\omega$ . Thus, the collective frequencies are given by  $\nu = \omega(2n + l)$ . In the isotropic case the variational ansatz leads to  $\alpha_0 = 1$  for  $P_0 = 0$ . Inserting this in (69), (72), (73) holds the following results:

$$\nu_{a,b,c} = 2\omega, \quad (81)$$

leading to the same quantum numbers as the limit  $P_0 \rightarrow \infty$ .

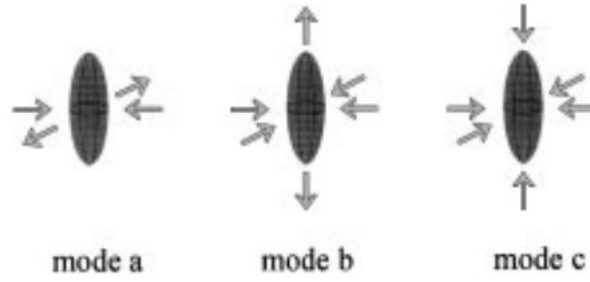


Figure 4: Oscillations modes of the condensate in a cylindrical trap [11].

## 2.4 Discussion

It may be useful to summarise what has been obtained so far.

The variational ansatz in this section leads to equations of motion for the widths of the condensate that can be solved in the vicinity of the equilibrium positions for small excitations. As already promised in the introduction, this resulted in a set of collective oscillation modes. Further examination showed that there are breathing and stretching modes. There is a certain number of equilibrium points depending on the interaction parameter  $P_0$  which was determined explicitly for spherical symmetry. Stable as well as unstable solutions can be detected and for a critical value of  $P_0$  there is no solution at all. This observation can be interpreted as a collapse of the condensate for  $P_0 < P_{\text{crit}}$ . This phenomenon has already been discovered in previous studies [17]. Using the definition (31) the value  $P_{\text{crit}}$  can be connected with a critical particle number.

Particular oscillation modes and their frequencies have been found and are illustrated in Figure 4. The 2D-quadrupole mode  $a$  in (64) with the frequency (59), the stretching mode  $b$  in (68) with the frequency (60) and the breathing mode  $c$  in (68) with the frequency (60).

In the two limits for the interaction  $P_0 \rightarrow \infty$  and  $P_0 \rightarrow 0$  the results are in good agreement with previous calculations. By inserting the values given in the experiment [16], the stretching mode oscillation frequency given by (68) can be compared with the Thomas-Fermi limit (76). For the given interaction strength  $P_0 \simeq 5$  the oscillation frequency is  $\nu_b \simeq 9.39$  Hz while the Thomas-Fermi limit leads to a frequency of  $\nu_{b,\text{TF}} \simeq 8.70$  Hz resulting in a variation of about 8%. Both frequencies are shown in Figure 5. We observe that the oscillation frequency converges rather slow for increasing  $P_0$  against the Thomas-Fermi limit.

## 3 Parametric Resonance

In this chapter the application of the parametric resonance to the collective oscillations of the condensate in the vicinity of the equilibrium positions will be discussed. This is done for the isotropic condensate but could be applied to other symmetries as well. The ansatz chosen here is based on the

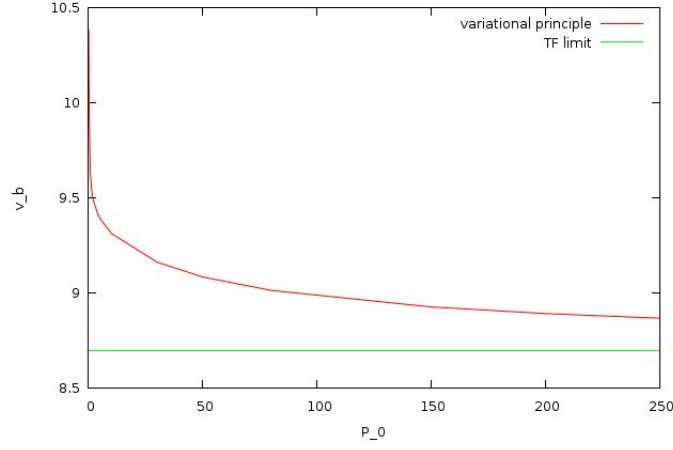


Figure 5: Oscillation frequency  $\nu_b$  of the stretching mode as a function of the interaction strength  $P_0$ . The red function is calculated by (68) while the green constant represents the frequency for the Thomas-Fermi limit (76), both calculated for the experiment parameters given in Ref. [16].

Mathieu equation

$$\ddot{x}(t) + [c - 2q \cos 2t] x(t) = 0. \quad (82)$$

First the dynamics of the condensate have to be rewritten in the form of the Mathieu equation, then a general solution for the equation and its characteristics can be determined and used to describe the special case of the condensate.

### 3.1 Spherical Trap

Again (47) will be used with a spherical trap symmetry, setting  $\lambda = 1$  and  $\alpha_{z0} = \alpha_0$ . In this case the constraints for the equilibrium points are given by (44). The potential for small excitations can be written as

$$V_{\text{eff}}(\alpha_0 + \delta\alpha) = V_{\text{eff}}(\alpha_0) + \frac{1}{2} \left[ 1 + \frac{3}{\alpha_0^4} + \frac{4P(\tau)}{\alpha_0^5} \right] \delta\alpha^2, \quad (83)$$

using (35) yields

$$V_{\text{eff}}(\alpha_0 + \delta\alpha) = V_{\text{eff}}(\alpha_0) + \frac{1}{2} \left[ 1 + \frac{3}{\alpha_0^4} + \frac{4P_0}{\alpha_0^5} + \frac{4P_1 \cos \frac{\Omega}{\omega} t}{\alpha_0^5} \right] \delta\alpha^2. \quad (84)$$

This leads to the following equation of motion for  $\delta\alpha$

$$\delta\ddot{\alpha}(t) + \left[ 1 + \frac{3}{\alpha_0^4} + \frac{4P_0}{\alpha_0^5} + \frac{4P_1 \cos \frac{\Omega}{\omega} t}{\alpha_0^5} \right] \delta\alpha = 0. \quad (85)$$

A rescaling of time

$$2t' = \frac{\Omega}{\omega}, \quad (86)$$

$$\frac{\partial}{\partial t} = \frac{\Omega}{2\omega} \frac{\partial}{\partial t'}, \quad (87)$$

brings (85) in the form of a Mathieu equation (82):

$$\delta\ddot{\alpha}(t') + \frac{4\omega^2}{\Omega^2} \left[ 5 - \frac{1}{\alpha_0^4} + \frac{4P_1 \cos 2t'}{\alpha_0^5} \right] \delta\alpha(t') = 0. \quad (88)$$

Comparing the coefficients with (82) leads to

$$c = \frac{4\omega^2}{\Omega^2} \left( 5 - \frac{1}{\alpha_0^4} \right), \quad (89)$$

$$q = -\frac{8P_1\omega^2}{\alpha_0^5\Omega^2}. \quad (90)$$

### 3.2 Pendulum

Another application of parametric resonance is a mathematical pendulum with oscillating centre of rotation. In this case the equation of motion can be linearised for small angles and results in a Mathieu equation as well. For a centre of rotation that oscillates with frequency  $\Omega$  and amplitude  $A$  the equation of motion is

$$\ddot{\varphi}(t) + \left( \frac{g}{l} + \frac{A\Omega^2}{l} \cos \Omega t \right) \sin \varphi(t) = 0, \quad (91)$$

where  $l$  denotes the length of the pendulum and  $\varphi(t)$  the angle. In analogy to the condensate in the spherical trap the equation of motion can be linearised for small oscillations around each equilibrium position  $\varphi_0 = 0, \pi$  and yields

$$\ddot{\varphi}(t) \pm \left[ \frac{g}{l} + \frac{A\Omega^2}{l} \cos \Omega t \right] \varphi(t) = 0. \quad (92)$$

Rescaling  $\varphi(t) = \tilde{\varphi} \left( \frac{2t'}{\Omega} \right)$ ,  $t' = \frac{\Omega t}{2}$  and comparing with (82) leads to

$$c = \pm \frac{4g}{l\Omega^2}, \quad q = \mp \frac{2A}{l} \quad (93)$$

with a positive  $c$  for the lower and a negative one for the upper equilibrium position. The parameter  $c$  depends on the frequency  $\Omega$  of the parametric oscillation, while  $q$  characterises the amplitude  $A$ .

### 3.3 Floquet Theory

In order to determine the behaviour of those systems described by the Mathieu equation (82) the Floquet theory can be used. This will result in a stability diagram depending on the parameters  $c$  and

$q$  as well as an equation for the resonance frequencies and a resonance curve corresponding to Figure 2 shown in the introduction. The Floquet theory says that for the Hill equation

$$\ddot{x}(t) + f(t)x(t) = 0 \quad (94)$$

with the property  $f(t) = f(t + T)$ , the solution can be written as

$$x(t) = u(t) e^{\lambda t}, \quad (95)$$

with  $u(t) = u(t + T)$ .

A similar theorem is often used in solid state physics known as Bloch theorem. The Bloch theorem makes a statement about the solutions of the Schrödinger equation for a spatially periodic potential.

Due to the solutions being periodic a fundamental system of solutions  $x_1(t), x_2(t)$  can be expressed by

$$\begin{pmatrix} x_1(t+T) \\ x_2(t+T) \end{pmatrix} = \begin{pmatrix} A_{11} & A_{12} \\ A_{21} & A_{22} \end{pmatrix} \begin{pmatrix} x_1(t) \\ x_2(t) \end{pmatrix}. \quad (96)$$

Further examination of the Wronski determinant of the fundamental system [14] shows that

$$\det \begin{pmatrix} A_{11} & A_{12} \\ A_{21} & A_{22} \end{pmatrix} = 1. \quad (97)$$

### 3.4 Fourier Series

Making use of the Floquet theory (95) the solutions can be described as a periodic part and a Floquet factor. Thus they can be expanded into a Fourier series

$$x(t) = \sum_{n=-\infty}^{\infty} x_n e^{(\lambda+2in)t}. \quad (98)$$

Inserting (98) in (82) leads to

$$\sum_{n=-\infty}^{\infty} x_n [(\lambda + 2in)^2 + c - 2q \cos 2t] e^{(\lambda+2in)t} = 0, \quad (99)$$

which can be rewritten as

$$\sum_{n=-\infty}^{\infty} \{x_n [(\lambda + 2in)^2 + c] - qx_{n-1} - qx_{n+1}\} e^{(\lambda+2in)t} = 0. \quad (100)$$

The equation has to hold for every  $t$  and  $n$ , so we conclude

$$x_n [(\lambda + 2in)^2 + c] - qx_{n-1} - qx_{n+1} = 0. \quad (101)$$

This is a trilinear recurrence relation for the Fourier coefficients  $x_n$ . The next step is to use this recurrence relation in order to find a relation between  $c$  and  $q$  for a given  $\lambda$ . It proves useful to define a set of ladder operators [19,20] to describe the relation between adjacent Fourier components:

$$x_{n-1} = S_n^- x_n, \quad (102)$$

$$x_{n+1} = S_n^+ x_n. \quad (103)$$

Using this in (101) yields

$$[(\lambda + 2in)^2 + c]x_n - q(S_n^- + S_n^+)x_n = 0, \quad (104)$$

which can be written as

$$x_{n+1} = \frac{1}{q}x_n[(\lambda + 2in)^2 + c] - S_n^- x_n. \quad (105)$$

Changing the indices from  $n \rightarrow n - 1$  leads to

$$x_n = \frac{1}{q}x_{n-1}[(\lambda + 2in)^2 + c] - S_{n-1}^- x_{n-1}. \quad (106)$$

Solving this for  $x_{n-1}$  yields

$$x_{n-1} = q\{[\lambda + 2i(n-1)]^2 + c - qS_{n-1}^- \}^{-1}x_n. \quad (107)$$

A comparison with (102) leads to the ladder operator

$$S_n^- = \frac{q}{[\lambda + 2i(n-1)]^2 + c - qS_{n-1}^-}. \quad (108)$$

Similar considerations result in an equation for the other operator

$$S_n^+ = \frac{q}{[\lambda + 2i(n+1)]^2 + c - qS_{n+1}^+}. \quad (109)$$

Both results (108), (109) together with (102), (103) can be inserted in the trilinear recurrence relation (101). Starting from  $n = 0$  leads to

$$\left[ \lambda^2 + c - \frac{q^2}{(\lambda + 2i)^2 + c - \frac{q^2}{(\lambda + 4i)^2 + c - \dots}} - \frac{q^2}{(\lambda - 2i)^2 + c - \frac{q^2}{(\lambda - 4i)^2 + c - \dots}} \right] x_0 = 0, \quad (110)$$

which consists of two continued fractions [20]. Since this equation has to hold even for  $x_0 \neq 0$  it connects the parameters  $\lambda$ ,  $q$  and  $c$ .

### 3.5 Stability Borders

In general solving this problem is quite difficult. Fortunately, the main interest lies within the stability of the oscillations for small parametric driving forces, i.e. small  $q$ . Thus the problem is to be solved by restricting it to the stability borders and small amplitudes  $q$ . By using (95) and (96) the periodic solutions of the Hill equation (94) can be written as a linear combination of  $x_1(t)$  and  $x_2(t)$ :

$$e^{\lambda T} [c_1 x_1(t) + c_2 x_2(t)] = c_1 [A_{11} x_1(t) + A_{12} x_2(t)] + c_2 [A_{21} x_1(t) + A_{22} x_2(t)]. \quad (111)$$

Since  $x_1(t), x_2(t)$  are linear independent of each other, this can be written as

$$\begin{pmatrix} A_{11} & A_{21} \\ A_{12} & A_{22} \end{pmatrix} \begin{pmatrix} c_1 \\ c_2 \end{pmatrix} = e^{\lambda T} \begin{pmatrix} c_1 \\ c_2 \end{pmatrix}. \quad (112)$$

The solutions of this eigenvalue problem are given by

$$e^{2\lambda T} - (A_{11} + A_{22}) e^{\lambda T} + \text{Det } A = 0, \quad (113)$$

which, due to (97), is solved by

$$e^{\lambda_{\pm} T} = \frac{\text{Tr } A \pm \sqrt{(\text{Tr } A)^2 - 4}}{2}, \quad (114)$$

with  $\text{Tr } A$  denoting the trace of the matrix  $A$ . By multiplying the two solutions it is easy to see that

$$\lambda_+ + \lambda_- = 0. \quad (115)$$

Combining (115) with (114) results in the stability borders. For  $\text{Tr } A > 2$  the exponents are real and no stable solution will be found. The condition  $\text{Tr } A < 2$  on the other hand leads to imaginary exponents and thus the stable solutions since the exponential function is bounded for pure imaginary exponents.

For  $q = 0$  the trace of  $A$  can be calculated straight-forwardly. With the two fundamental solutions  $x_{1/2}(t) = e^{\pm i\sqrt{c}t}$  and (97) the stability borders can be found at

$$c_n = n^2, \quad (116)$$

with  $n$  being an integer.

Inserting (116) in (93) leads to the resonance frequencies

$$\omega_n = \frac{2\omega_0}{n}, \quad (117)$$

where  $\omega_0$  is the oscillation frequency of the undisturbed system (for example the linearised pendulum) for small oscillations. Now that the stability borders are given with  $\lambda = \pm i\sqrt{c}$  and (116), the continued fractions in (110) can be expanded at those points up to the desired order in  $q$ .

For  $\lambda = 0$  we obtain

$$c - \frac{2q^2}{-4 + c - \frac{q^2}{-16+c-\dots}} = 0. \quad (118)$$

This problem can be solved for small  $q$  with the ansatz  $c(q) = a_0 + a_1q + a_2q^2 + \dots$ . Evaluating the continued fractions by only considering terms up to second order in  $q$  leads to

$$a_1q + a_2q^2 - \frac{2q^2}{-4 + a_1q + a_2q^2 + \dots} = 0, \quad (119)$$

which yields

$$c_0(q, \lambda = 0) = -\frac{1}{2}q^2 + \dots \quad (120)$$

The same procedure can be applied for  $\lambda = \pm i$  as well as  $\lambda = \pm 2i$ . The resulting stabilities are illustrated in Figure 6 and the corresponding functions are [21]:

$$c_1^- = 1 - q - \frac{1}{8}q^2 + \dots, \quad (121)$$

$$c_1^+ = 1 + q - \frac{1}{8}q^2 + \dots, \quad (122)$$

$$c_2^- = 4 - \frac{1}{12}q^2 + \dots, \quad (123)$$

$$c_2^+ = 4 + \frac{5}{12}q^2 + \dots \quad (124)$$

These results are obtained by taking into account the following technical problem. While expanding the continued fractions, resonances may appear for certain values of  $\lambda$ . Here this phenomenon is shown by the example of the ansatz  $c_1 = 1 + b_1q + b_2q^2 + \dots$  inserted in (110) for  $\lambda = i$ :

$$i^2 + 1 + b_1q + b_2q^2 - \frac{q^2}{(3i)^2 + 1 + b_1q + b_2q^2 + \dots} - \frac{q^2}{(-i)^2 + 1 + b_1q + b_2q^2 + \dots} = 0, \quad (125)$$

which results in

$$b_1q + b_2q^2 + \frac{q^2}{8 + \dots} - \frac{q^2}{b_1q + \dots} = 0. \quad (126)$$

Thus a thorough investigation of the continued fractions for each expansion is necessary in order not to miss crucial terms.

In the case of the pendulum the values of  $c > 0$  correspond to the stable equilibrium position while the unstable region with  $c < 0$  corresponds to the upper equilibrium position. For  $q > 0$  this equilibrium point can be stabilised which can be seen by the functions crossing the  $x$ -axis. The expressions derived for the stability borders and the diagram are now used for the condensate as well. For the condensate inserting the corresponding expressions for  $c$  in (89) and  $q$  in (90) in (120) leads to

$$P_1 = \sqrt{\frac{\alpha_0^{10}}{8} \left( \frac{1}{\alpha_0^4} - 5 \right)} \frac{\Omega}{\omega}, \quad (127)$$

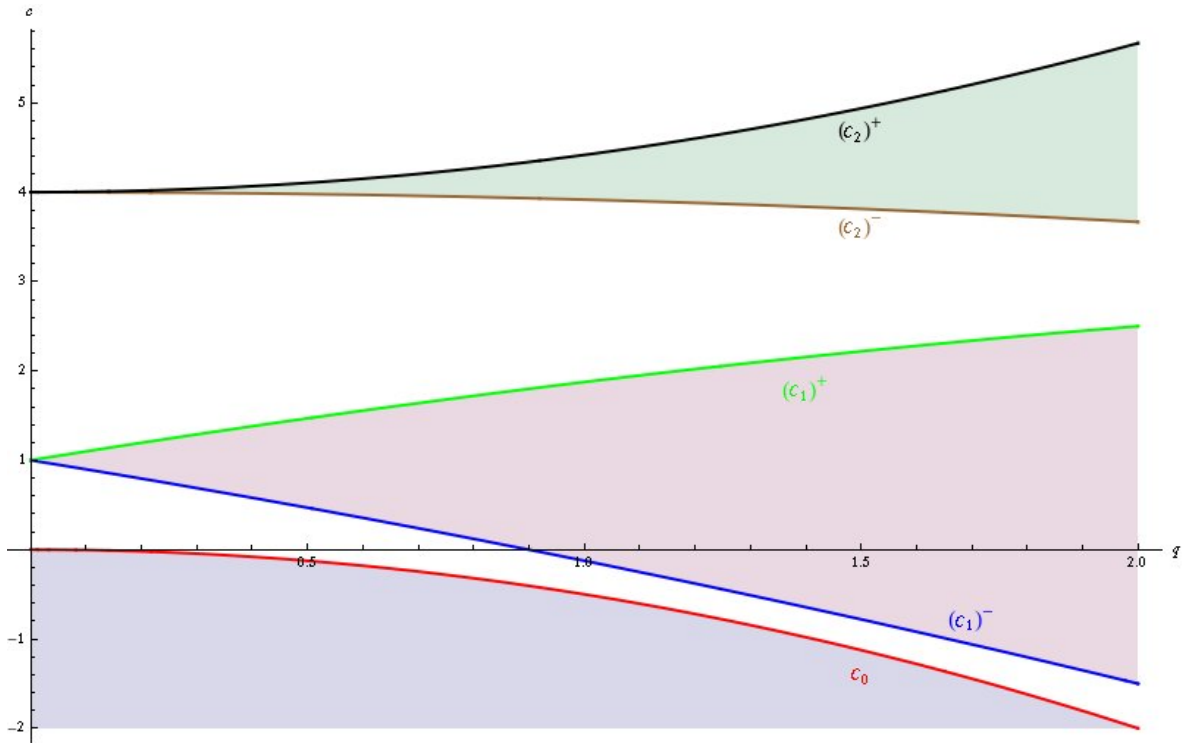


Figure 6: Stability diagram for the Mathieu equation. The coloured functions are the stability borders (120)–(124) calculated for small  $q$ . The filled regions denote unstable oscillations.

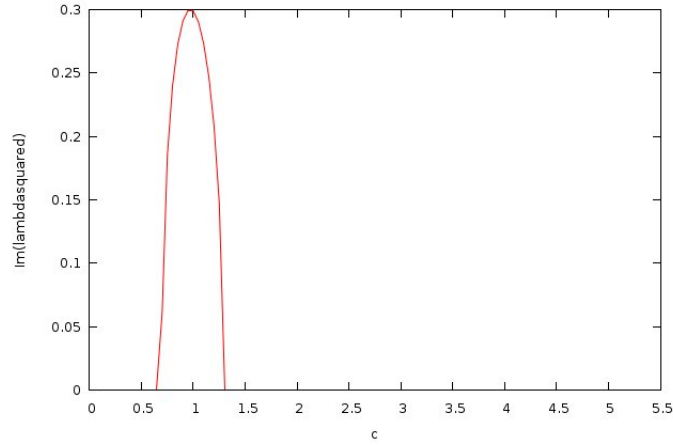
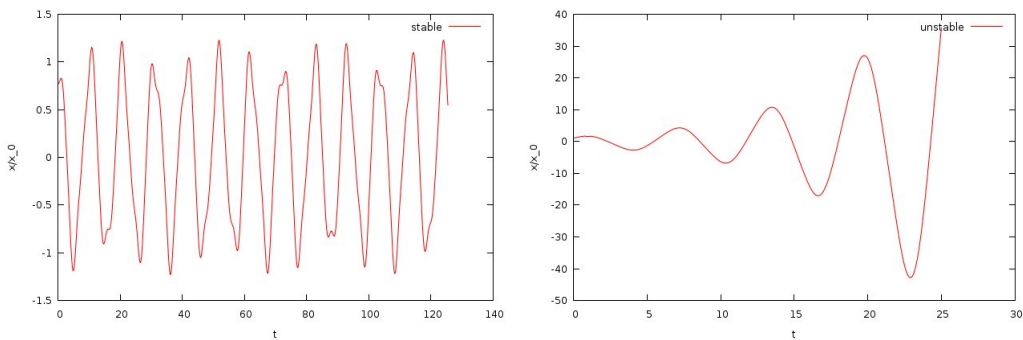
which describes the relation between modulation frequency  $\Omega$  and interaction strength  $P_1$  for the stabilisation of the breathing mode. Inserting the parameters in (116) and using (73) for the eigenfrequency of the breathing mode it is possible to reproduce (117). Thus the resonances are expected to occur at twice the eigenfrequency divided by an integer.

### 3.6 Resonance Curves

In order to compare our findings to the experimental results of Figure 2 it is necessary to calculate the solutions of the Mathieu equation defined by (98). Comparing with Section 3.1 shows that the solutions  $x(t)$  correspond to the variation of the variational width parameter  $\delta\alpha$ . Again the plan is to first calculate a general solution for the Mathieu equation and then specialise to the trapped condensate by inserting the parameter definitions (89) and (90). First of all the behaviour of  $\lambda$  for a fixed  $q$  has to be determined. The Floquet exponent  $\lambda$  is given as a function of  $c$  and  $q$  by (110). Rewriting this equation and expanding the continued fractions only up to the first denominator results in a polynomial of third grade in  $\lambda^2$ :

$$16c - 8c^2 + c^3 + 8q^2 - 2cq^2 + \lambda^2(16 + 3c^2 - 2q^2) + \lambda^4(8 + 3c) + \lambda^6 = 0. \quad (128)$$

Solving this equation by using the Cardano formulas [22] results in 3 solutions for  $\lambda^2$ . However, for  $q = 0$  the solution has to fulfil  $\lambda^2 = -c$ . Since the expansion only holds for small  $q$ , this condition can be used to determine the relevant solution. For a fixed  $q > 0$  the squared Floquet exponent becomes


 Figure 7: Imaginary part of  $\lambda^2$  solving (128) as a function of  $c$ .

 Figure 8: Time signal  $x/x_0$  for fixed  $q = 0.3$ . The left plot shows a stable oscillation calculated for  $c = 0.3$  while the function shown in the right plot with  $c = 1$  is divergent. The latter unstable behaviour corresponds to the Floquet exponent  $\lambda$  shown in Figure 7.

complex around certain values of  $c$ . This behaviour is shown in Figure 7.

Choosing the sign when taking the square root determines if the oscillation diverges or converges. The solution for  $\lambda$  has to be inserted into the Fourier series (98). Around  $n = 0$  this results in

$$\frac{x}{x_0} = e^{\lambda t} \left[ 1 + e^{2it} \frac{q}{(\lambda + 2i)^2 + c} + e^{-2it} \frac{q}{(\lambda - 2i)^2 + c} \right]. \quad (129)$$

For a fixed value of  $q$  the relative amplitude  $\frac{x}{x_0}$  is a function of  $t$  and  $c$ . With regard to Figure 7 a resonance is expected to be seen around  $c = 1$ . The time signal for this value is plotted in Figure 8 and compared to the time signal for another value of  $c$  where  $\lambda$  does not show any odd behaviour. Since  $x/x_0$  is oscillating with different phases for every  $c$  it is necessary to determine the maximum in an appropriate time interval. Evaluating the continued fractions in second and higher orders leads to polynomials of higher degree in  $\lambda^2$ . For every denominator the degree is increased by two, thus the equations have to be solved numerically. Solving (110) for higher orders and inserting into

$$x(t) = x_0 e^{\lambda t} (1 + e^{2it} S_1^+ + e^{-2it} S_1^- + \dots) \quad (130)$$

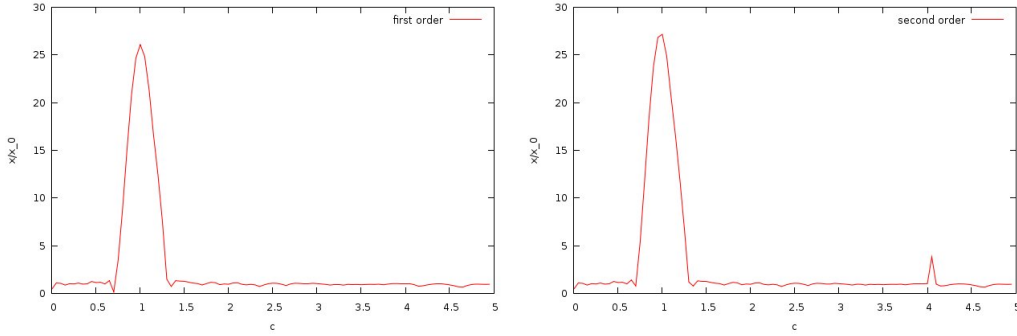


Figure 9: Resonance spectrum for the Mathieu equation calculated by expanding the continued fractions up to the first (left plot) and second denominator (right plot).

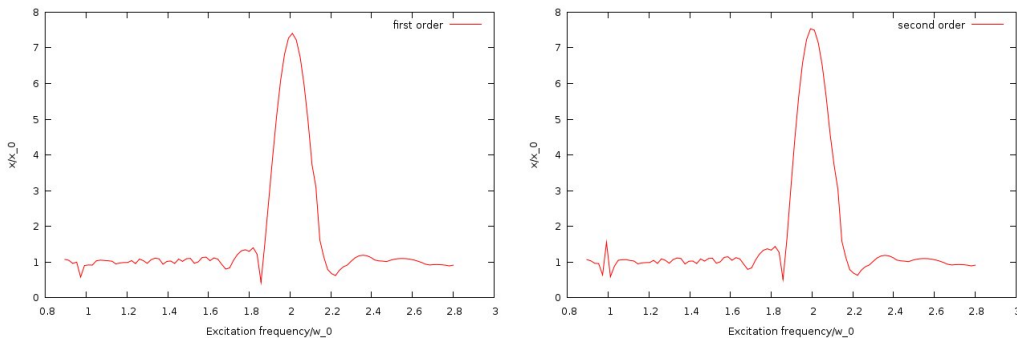


Figure 10: Resonance spectrum of the condensate in a spherical trap in first and second order. The maximal amplitude in a time interval is plotted over the modulation frequency.

leads to further resonances at higher values of  $c$  corresponding to the integer  $n$  due to (117). The maximal elongation in a specific time interval for  $q = 0.3$  has been plotted in Figure 9 over  $c$  for expansion in first and second order. The first resonance can be seen at  $c = 1$  and corresponds to the value of  $n = 1$  and the second appears at  $c = 4$ ,  $n = 2$ . In both plots the first resonance can be seen. With a difference of less than 5% the height of the resonance peak does not significantly change from first to second order, thus justifying our approximative procedure. Furthermore the drastic difference in the peak heights shows that the first resonance is stronger than the second one. It can be expected that the third resonance is even weaker.

By using (89) and (90) again the amplitude corresponding to the variational width  $\delta\alpha$  becomes a function of  $t$  and  $\Omega$  since all parameters  $c$ ,  $q$  and  $\lambda$  are functions of  $\Omega$ . Corresponding to the experiment the maximum amplitude around a specific time-interval has been calculated and plotted over the relative modulation frequency  $\frac{\Omega}{\omega_0}$  in Figure 10, where the amplitude is shown for an expansion of the continued fractions up to the second denominator.

Figure 10 corresponds qualitatively to the characteristics of parametric and to observations made in other applications like the swing, where the resonance effect is maximal at twice the oscillation frequency. Just as in Figure 9 the change in height of the first resonance peak between the first and

---

second order is less than 5%. The factor of height difference between the first ( $\sim 6.6$ ) and the second ( $\sim 1.6$ ) resonance peak shown in the right plot is about 10. Further resonances are expected to be seen at lower frequencies due to (117) and could be calculated by further expanding the continued fractions. Presuming that the height difference factor between third and second resonance is about the same as between second and first, it would be impossible to identify any further resonances.

Contrary to Figure 2 the resonance peak at the lower frequency in Figure 10 is much smaller than the other one, while the experiment data shows a small peak at a high frequency and a big one at the lower frequency. However, there is a difference between the experimental setup and our theoretical considerations regarding the trap symmetry. While the theoretical studies of this work are based on the breathing mode of the condensate confined by a spherical trap in the experiment a quadrupole mode of a cylindrical condensate was examined, the latter depends crucially on the anisotropy of the condensate. It remains to be investigated whether the qualitative differences between the resonance spectra of Figures 2 and 10 are really due to the different trap geometries.

## 4 Summary and Conclusion

In this work the dynamics of a trapped Bose-Einstein condensate have been studied by using a variational approach [11]. Additionally the phenomenon of parametric resonance has been discussed and a general approach for studying systems with dynamics that can be expressed by a Mathieu equation has been introduced. While parametric resonance is a common phenomenon with applications such as the Paul trap or the acceleration of a swing, it has not been successfully used for a stabilisation or destabilisation of the condensates collective oscillations until now.

The current experiment led by V.S. Bagnato and R.G. Hulet [16] is a first step in this direction. Due to the complexity of the problem the results presented in this work have been calculated for a spherical trap. In the experiment, however, a cylindrical trap is used, which might be the reason for the differences between the resonance spectra presented in Figure 2 and Figure 10. The resonance curve calculated by solving the Mathieu equation clearly shows the expected characteristics of parametric resonance, a main peak at twice the eigenfrequency and smaller peaks at smaller frequencies defined by (117). In the experimental data for the cylindrical trap the peak heights are interchanged which contradicts not only the calculations in this work but also the results for other parametric driven systems such as the swing. In order to study this discrepancy the approach made here has to be generalised for cylindrical symmetry which leads to matrix-valued continued fractions [20].

## References

- [1] S.N. Bose, *Plancks Gesetz und Lichtquantenhypothese*, Zeitschrift für Physik **26**, 178 (1924)
- [2] A. Einstein, Sitz. Ber. Preuss. Akad. Wiss. (Berlin) **22**, 261 (1924)

- [3] E. Cornell, C. Wieman, M. Matthews, M. Anderson, and J. Ensher, *Observation of Bose-Einstein Condensation in a Dilute Atomic Vapor*, Science **269**, 198 (1995)
- [4] K. Davis, M. Mewes, M. Andrews, W. Ketterle, D. Kurn, D. Durfee, and N. Vandruten, *Bose-Einstein Condensation in a Gas of Sodium Atoms*, Phys. Rev. Lett. **75**, 3969 (1995)
- [5] L.P. Pitaevskii and S. Stringari, *Bose-Einstein Condensation*, Oxford Science Publications (2003)
- [6] C.J. Pethick and H. Smith, *Bose-Einstein Condensation in Dilute Gases*, Cambridge University Press (2002)
- [7] A. Griffin, D.W. Smoke, and S. Stringari, *Bose-Einstein Condensation*, Cambridge University Press (1995)
- [8] H.T.C. Stoof, K.B. Gubbels, and D.B.M. Dickerscheid, *Ultracold Quantum Fields*, Springer (2009)
- [9] D.M. Stamper-Kurn, H.-J. Miesner, S. Inouye, M.R. Andrews, and W. Ketterle, *Collisionless and Hydrodynamic Excitations of a Bose-Einstein Condensate*, Phys. Rev. Lett. **81**, 500 (1998)
- [10] S. Stringari, *Collective Excitations of a Trapped Bose-Condensed Gas*, Phys. Rev. Lett. **77**, 2360 (1996)
- [11] V.M. Perez-Garcia, H. Michinel, J.I. Chirac, M. Lewenstein, and P. Zoller, *Low Energy Excitations of a Bose-Einstein Condensate: A Time-Dependent Variational Analysis*, Phys. Rev. Lett. **77**, 5320 (1996).
- [12] V.M. Perez-Garcia, H. Michinel, J.I. Chirac, M. Lewenstein, and P. Zoller, *Dynamics of Bose-Einstein condensates: Variational solutions of the Gross-Pitaevskii equations*, Phys. Rev. A **56**, 1424 (1997)
- [13] R.G. Hulet, Y.P. Chen, S.E. Pollack, D. Dries, M. Junker, and T.A. Corcovilos, *Extreme Tunability of Interactions in a  $^7\text{Li}$  Bose-Einstein Condensate*, Phys. Rev. Lett. **102**, 090402 (2009)
- [14] A. Pelster, *Theoretische Mechanik*, Skript zur Vorlesung in den Wintersemestern 2000/2001 und 2001/2002, <http://users.physik.fu-berlin.de/~pelster/Manuscripts/mechanik.pdf>
- [15] W. Paul and H. Steinwedel, *Ein neues Massenspektrometer ohne Magnetfeld*, Zeitschrift für Naturforschung A **8**, 448 (1953)
- [16] K.M.F. Magalhaes, E.R.F. Ramos, M.A. Caranhanas, V.S. Bagnato, D. Dries, S.E. Pollack, and R.G. Hulet, *Collective Excitation of a Trapped Bose-Einstein Gas by Modulation of the Scattering Length*, in preparation
- [17] F.K. Abdullaev, R. Galimzyanov, M. Brtka, and R. Kraenkel, *Resonances in a trapped 3D Bose-Einstein condensate under periodically varying atomic scattering length*, J. Phys. B **37** (2004)
- [18] F. Abdullaev, *Nonlinear Matter Waves In Cold Quantum Gases*, International Islamic University Malaysia (2005)
- [19] C. Simmendinger, *Untersuchung von Instabilitäten in Systemen mit zeitlicher Verzögerung*, Diplomarbeit, Universität Stuttgart, 1995

- [20] H. Risken, *The Fokker-Planck Equation: Methods of Solution and Applications*, Springer (1996)
- [21] M. Abramowitz and I.A. Stegun (Editors), *Handbook of Mathematical Functions with Formulas, Graphs and Mathematical Tables*, National Bureau of Standards Applied Mathematics, Washington, 1964
- [22] W. Greiner, *Mechanik Teil 2*, Harri Deutsch (1998)

## **Commitment**

This is to certify that I wrote this work on my own and that the references include all the sources of information I have utilised.

Berlin, September 30th 2009

Jochen Brüggemann